In-silico design and ADMET predictions of some new imidazo[1,2-a]pyridine-3-carboxamides (IPAs) as anti-tubercular agents

Mustapha Abdullahi [a,*], Niloy Das [b], Shola Elijah Adeniji [c], Alhassan Kabiru Usman [a], Ahmad Muhammad Sani [a]

[a] Faculty of Sciences, Department of Pure and Applied Chemistry, Kaduna State University, Tafawa Balewa Way, Kaduna State, Nigeria
[b] Department of Pharmacy, BGC Trust University Bangladesh, Chittagong 4381, Bangladesh
[c] Faculty of Physical Sciences, Department of Chemistry, Ahmadu Bello University, P.M.B. 1044 Zaria, Kaduna State, Nigeria

ARTICLE INFO

ABSTRACT

Tuberculosis (TB) is one of the leading infectious diseases worldwide even with the ravaging COVID-19 pandemic in recent times. This mandated further search and exploration of more possible anti-TB drug candidates against *M. tuberculosis* strains. As an extension of our previous work on the homology modeled cytochrome *b* subunit of the bc1 complex (QcrB) of Mycobacterium tuberculosis, an in-silico design was carried out in order to further explore more newly potential anti-TB compounds. Ligand 26 was selected as the lead template (scaffold A) based on our previous docking results and its less bulky structure. Successively, eight (8) new ligands (A1–A8) were designed with better binding affinities in comparison to the scaffold template (−6.8 kcal/mol) and isoniazid standard drug (−6.00 kcal/mol) respectively. In addition, three (3) designed ligands namely, **A6, A2, and A7** with higher binding affinities were validated via ADME and toxicity prediction analysis, and the results showed zero violations of Lipinski rules with similar bioavailability, and high rate in gastrointestinal absorption, while toxicity parameters such as carcinogenicity and cytotoxicity were all predicted as non-toxic (inactiveness). The designed IPA compounds in the present study could serve as a promising gateway that could help the medicinal and synthetic chemist in the exploration of a new set of derivatives as anti-TB agents. Therefore, this research strongly recommends further experimental consideration of the newly designed IPA compounds through synthesis, in-vitro and in-vivo studies to validate the theoretical findings.

1. Introduction

Mycobacterium tuberculosis is the organism that causes one of the chronic infectious diseases popularly known as Tuberculosis (TB) responsible for the global high mortality rate [1]. The emergence of the severe acute respiratory syndrome coronavirus 2 (SARS-CoV-2) as the cursor of the COVID-19 pandemic has continued to dominate the scientific research community and other media outlets in recent times [2,3]. Scientific evidence based on clinical perspective indicates that COVID-19 materializes regardless of TB manifestation, either after, during, or before an active diagnosis [2]. Therefore, TB should be given utmost attention even with its global declining rate of cases [1]. An imidazo [1, 2-a] pyridine-3-carboxamide (IPA) candidate (Q203) was reported to exhibit robust inhibitory activity against extensively drug-resistant (XDR) and multidrug-resistant (MDR) strains and it is currently in clinical trials [4]. Researchers are currently developing a

keen interest in the synthesis of diverse series of compounds as anti-TB agents. Recently, benzo[d]imidazole-2-carboxamides and benzimidazoquinazoline derivatives as new anti-TB agents were designed, synthesized, and tested for biological responses respectively [5,6]. Hence, the rapid increase in the occurrences of TB drug resistance attracts the need to find new therapeutics as well to discover novel drug targets that could effectively kill *M. tuberculosis* when exploited. Some of the promiscuous targets inhibited by more than one compound include DprE1, MmpL3, QcrB, etc [7]. The novel derivatives of Q203 (IPAs) as anti-TB agents were also reported to have the ability to block the growth of MDR and XDR strains of *M. tuberculosis* by targeting the respiratory cytochrome bc1 complex (QcrB) [7]. The QcrB subunit is an important component of the electron transport chain necessary for the synthesis of ATP as it catalyzes the transfer of an electron from the ubiquinol to the cytochrome *c* [8]. However, the interaction of bonded ligand to the QcrB subunit receptor remains unclear and the crystal structure is not

* Corresponding author.
  E-mail address: mustychem19@gmail.com (M. Abdullahi).

available in the Protein Data Bank (PDB) [9]. The search for more potent compounds is very tedious, costly, and time-consuming [10]. As such, the use of computational chemistry tools based on theoretical insights could come in handy with the aim to modify and design new compounds with better bioactivities. Some of the computational methods employed in computer-aided drug design include homology modeling, molecular docking simulation, pharmacokinetic predictions, and QSAR analysis amongst others. These computational approaches have been employed over the years to improve existing anti-tubercular agents through virtual screening for the identification and modification of potential hits [11,12]. Structure-based drug design (SBDD) solemnly depends on the knowledge and information of the 3D crystal structure of the targeted

protein to design the ligands that can serve as better inhibitors [13]. In the case where the 3D experimental structure of the targeted protein is not reported, the experimental amino acid sequence can be used to build a homology model [14]. The homology modeling technique predicts the 3D structure of the targeted protein sequence based on the alignment of an experimentally known homologous protein as a template [15]. In our previous report, homology modeling and molecular docking studies were carried out on some IPAs anti-TB agents targeting the QcrB sub-unit. The homology modeling of the receptor built and predicted a new 3D structure of QcrB target in M. tuberculosis using QcrB subunit of *M. smegmatis* as template [12,16]. Furthermore, the results of molecular docking in the study further revealed the binding profiling of the 35 IPA

Table 1

Chemical structures of the designed imidazo[1,2-a] pyridine-3-carboxamides (IPAs).
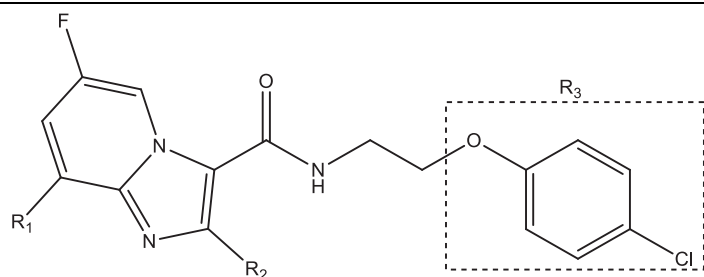
Template scaffold A (−6.8 kcal/mol)

Compound code	R_1	R_2	R_3
A1	Cl	Me	
A2	Cl	Me	
A3	H	Me	
A4	H	Et	
A5	H	Me	
A6	H	n-Pr	
A7	H	OMe	
A8	H	c-Pr	

ligands docked with the modeled protein. In the current study, the same 3D crystal structure of the QcrB modeled protein in *M. tuberculosis* was used to analyze the binding profiling and ADMET prediction of some newly designed compounds as potential hits of anti-TB candidates.

2. Methodology

2.1. Template selection and structural modifications

In our previous report, we have successfully carried out virtual screening of thirty-five (35) N-(2-phenoxy) ethyl imidazo[1,2-a] pyridine-3-carboxamides (IPAs) synthesized by Wang et al., (2019) with our homology modeled QcrB protein as the active target in the *Mycobacterium tuberculosis* [7,16]. As such, ligand 26 was selected as the template scaffold for further structural modification and rigorous molecular docking simulation. The structure of the newly designed ligands was drawn (Table 1) and optimized accurately at the density functional level of theory (B3LYP/6-31G**) in a vacuum using Spartan 14 [17].

2.2. Molecular docking, ADME analysis, and toxicity prediction

Molecular docking is the most preferable technique in structure-based drug design to predict the binding free energy and the binding mode of the protein and ligand compound [18]. Therefore, molecular docking simulation was carried out to determine the binding affinities and the residual interactions when the ligand molecules bind with the active pockets of the protein as macromolecule using AutoDock 4.2 module implemented in PyRx 0.8. Blind docking was performed for all the designed ligand molecules to predict the active binding pockets of the modeled QcrB protein as the targeted macromolecule [19]. To ensure that all ligand molecules are properly docked, the 3D grid box dimensions were adjusted as X: 203.60, Y: 177.43, Z: 211.23 for grid center, and X: 88.26, Y: 86.09, Z: 82.38 for the number of points at the spacing of 1.875 Å on the whole protein structure to predict the best outcome of the docking task. Furthermore, the docking algorithm used was the Lamarckian Genetic Algorithm at default parametrized settings. After docking, protein and the ligands were obtained in PDBQT format, and complexes were formed using UCSF Chimera software while the visualization of residual interactions was done using Discovery Studio 2020 and UCSF Chimera software accordingly. The Swiss ADME online server (http://www.swissadme.ch/) was applied to predict absorption, distribution, metabolism, and excretion properties of the best ligands while ProTox-II online server (https://tox-new.charite.de/protox_II/) was also used to determine their toxicity.

3. Results and discussions

3.1. Molecular docking analysis

The docking results of ligand molecules with the targeted protein showed the binding affinity ranging from (−8.5 kcal/mol to −11 kcal/mol). To compare the best binding affinity of the ligand molecules, we docked the standard drug with the modeled QcrB protein in *M. tuberculosis* and showed binding affinity as (−6.00 kcal/mol). All binding amino acid residues including non-bond interactions and binding affinities of the stable complexes formed were shown in Table 2.

A6 showed the best binding affinity (−11.0 kcal/mol) as a complex with the respected modeled QcrB protein and formed one conventional hydrogen bond with the amino acid residue of (GLY62 at a distance of 2.39142 Å) and Halogen (Fluorine), Amide-Pi Stacked, Alkyl, Pi-Alkyl bonds with the amino acid residues of (LEU58, LEU59, VAL63, ILE217, LEU65, LEU166, PRO167, PRO221, PHE69, TYR213) showed in Fig. 1. The complex of the **A2** ligand molecule with the targeted modeled QcrB protein showed (−10.5 kcal/mol) binding affinity and formed one Conventional Hydrogen Bond with the amino acid residue (GLY62 at a distance of 2.08894 Å). Four different types of bonds such as Halogen

Table 2
Binding affinity (kcal/mol) and non-bonding interactions of the complexes.

Compounds	Binding affinity (kcal/mol)	Bonding types	Interacting amino acid residues	Distance (Å)
Standard drug	−6.00	Conventional Hydrogen Bond	LEU58	2.09388
		Conventional Hydrogen Bond	LEU59	2.84072
		Pi-Anion	GLU159	3.32022
		Pi-Alkyl	LEU58	3.97204
		Pi-Alkyl	PRO221	5.18191
A1	−8.5	Conventional Hydrogen Bond	ALA385	2.52924
		Halogen (Fluorine)	LEU348	2.87618
		Pi-Sigma	PHE133	3.61502
		Pi-Sigma	ALA385	3.67506
		Pi-Sigma	ALA385	3.60692
		Pi-Pi T-shaped	PHE133	4.99664
		Amide-Pi Stacked	ALA385	4.12602
		Amide-Pi Stacked	ILE386	4.12602
		Alkyl	LEU129	5.40777
		Alkyl	ILE386	4.18787
		Alkyl	VAL345	4.30783
		Alkyl	ALA385	4.43333
		Alkyl	ALA385	4.32462
		Pi-Alkyl	ILE386	5.06303
		Pi-Alkyl	LEU129	5.19201
		Pi-Alkyl	PHE133	4.1159
		Pi-Alkyl	PHE134	4.35564
		Pi-Alkyl	PHE388	4.7971
		Pi-Alkyl	TYR389	4.44871
A2	−10.5	Conventional Hydrogen Bond	GLY62	2.08894
		Halogen (Fluorine)	GLU159	3.59989
		Pi-Anion	GLU159	4.31326
		Alkyl	LEU59	3.92938
		Alkyl	PRO221	4.39931
		Alkyl	LEU65	4.57881
		Alkyl	ARG111	4.54332
		Alkyl	PRO167	4.47863
		Alkyl	LEU65	4.48087
		Alkyl	LEU166	5.41423
		Alkyl	PRO167	5.16489
		Pi-Alkyl	ILE217	4.59328
		Pi-Alkyl	PRO221	4.71614
		Pi-Alkyl	PHE69	5.14437
		Pi-Alkyl	PHE69	4.72374
A3	−10.0	Halogen (Fluorine)	HIS114	3.36308
		Pi-Anion	GLU159	3.94788
		Alkyl	LEU58	3.81904
		Alkyl	LEU59	4.09035
		Alkyl	PRO221	4.4197
		Alkyl	LEU65	4.40346
		Alkyl	LEU166	4.97691
		Pi-Alkyl	LEU58	5.39169
		Pi-Alkyl	LEU59	5.27014
		Pi-Alkyl	PRO221	4.32695
		Pi-Alkyl	PHE69	4.72942
		Pi-Alkyl	HIS114	5.15802
		Pi-Alkyl	HIS216	5.28912
A4	−9.1	Carbon Hydrogen Bond	GLY163	3.31031
		Halogen (Fluorine)	GLY163	3.31031
		Halogen (Fluorine)	HIS114	3.68598
		Halogen (Fluorine)	HIS216	3.05615
		Pi-Sigma	LEU65	3.7055
		Alkyl	ALA97	3.69526
		Alkyl	ILE100	4.33314
		Alkyl	ARG111	4.58662
		Alkyl	PRO167	4.85181

Table 2 (*continued*)

Compounds	Binding affinity (kcal/mol)	Bonding types	Interacting amino acid residues	Distance (Å)
		Alkyl	ILE217	4.56014
		Alkyl	PRO221	5.48313
		Pi-Alkyl	PRO167	5.10454
		Pi-Alkyl	PHE69	5.29162
		Pi-Alkyl	HIS114	4.68175
		Pi-Alkyl	HIS216	5.24304
A5	−10.3	Halogen (Fluorine)	HIS114	3.50679
		Alkyl	LEU58	4.04364
		Alkyl	PRO221	4.89791
		Alkyl	LEU65	4.70392
		Alkyl	ILE217	5.46661
		Alkyl	LEU65	4.52788
		Alkyl	LEU65	4.86007
		Alkyl	LEU166	4.60995
		Alkyl	PRO221	5.42632
		Pi-Alkyl	LEU59	5.39063
		Pi-Alkyl	PRO221	4.44757
		Pi-Alkyl	PHE69	4.87213
		Pi-Alkyl	HIS114	5.14963
		Pi-Alkyl	HIS114	5.12793
		Pi-Alkyl	HIS216	5.28053
A6	−11.0	Conventional Hydrogen Bond	GLY62	2.39142
		Halogen (Fluorine)	GLU159	3.66252
		Amide-Pi Stacked	LEU58	4.97455
		Amide-Pi Stacked	LEU59	4.97455
		Alkyl	LEU58	4.97214
		Alkyl	VAL63	4.49813
		Alkyl	ILE217	4.54423
		Alkyl	LEU65	4.95044
		Alkyl	LEU166	5.47454
		Alkyl	LEU65	4.41666
		Alkyl	PRO167	5.21434
		Alkyl	PRO221	4.89313
		Pi-Alkyl	ILE217	4.84499
		Pi-Alkyl	PHE69	5.17173
		Pi-Alkyl	PHE69	5.12895
		Pi-Alkyl	TYR213	5.39932
A7	−10.5	Carbon Hydrogen Bond	HIS216	3.78978
		Halogen (Fluorine)	HIS114	3.60387
		Alkyl	LEU58	4.03498
		Alkyl	LEU59	3.97007
		Alkyl	LEU65	5.01232
		Alkyl	LEU65	4.53948
		Alkyl	PRO167	5.11711
		Alkyl	PRO221	5.46251
		Pi-Alkyl	LEU59	5.39657
		Pi-Alkyl	PRO221	4.5088
		Pi-Alkyl	PHE69	5.20022
		Pi-Alkyl	HIS114	5.13828
		Pi-Alkyl	HIS114	4.95511
		Pi-Alkyl	HIS216	5.23027
		Pi-Alkyl	HIS216	5.00678
A8	−9.0	Conventional Hydrogen Bond	ALA385	2.16555
		Amide-Pi Stacked	ALA385	4.63904
		Amide-Pi Stacked	ILE386	4.63904
		Alkyl	LEU129	4.97501
		Alkyl	MET126	4.10023
		Alkyl	VAL345	4.66888
		Alkyl	VAL345	4.80002
		Alkyl	LEU348	5.44256
		Alkyl	ALA385	4.26799
		Alkyl	ALA385	4.0649
		Alkyl	ALA385	4.78506
		Pi-Alkyl	LEU129	5.14748
		Pi-Alkyl	ALA385	4.62964
		Pi-Alkyl	ILE386	4.76785
		Pi-Alkyl	PHE133	4.51175
		Pi-Alkyl	PHE388	4.91468
		Pi-Alkyl	TYR389	3.85255
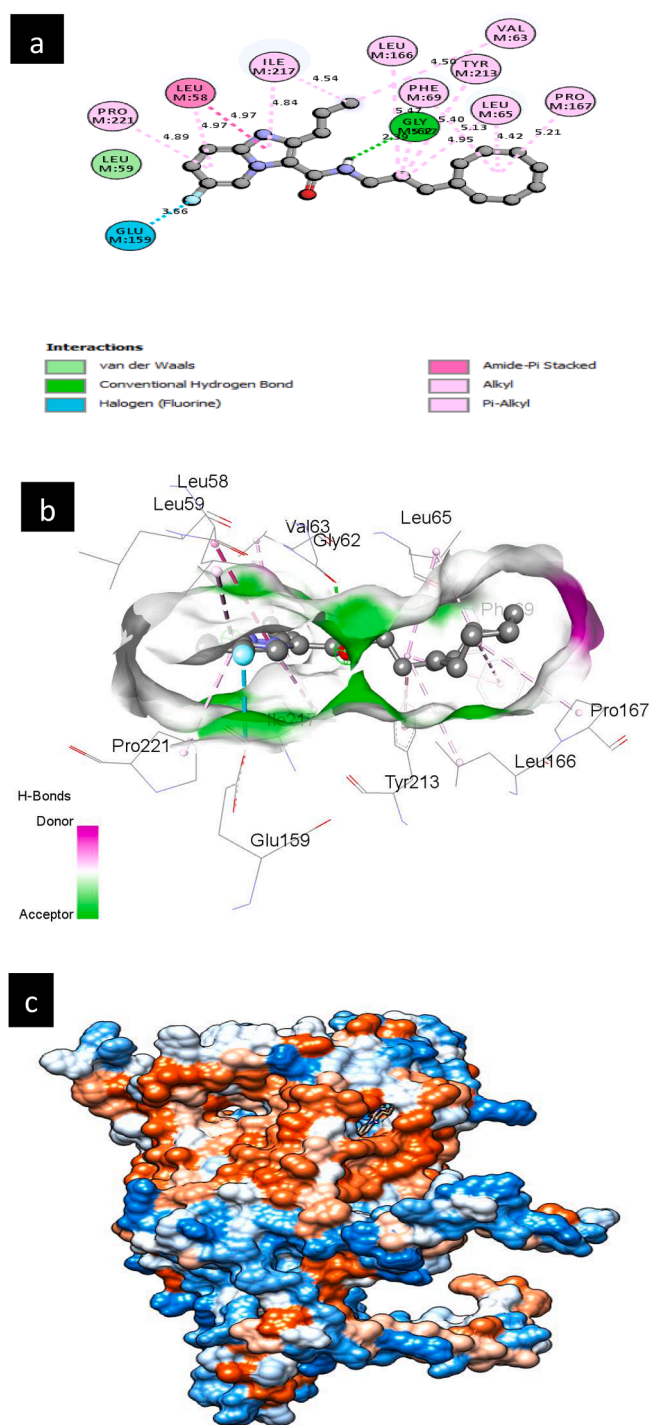
Fig. 1. (a) Schematic representation of predicted **A6** ligand with protein complex interactions in the 2D diagram. Interactions are colored depending on their type. (b) The three-dimensional representation of the binding pose, interactions, H bond donor, and acceptor surface of predicted **A6** ligand with the protein complex. (c) Targeted protein is depicted in surface view and **A6** ligand compound as the stick in the binding pocket.

(Fluorine), Pi-Anion, Alkyl, Pi-Alkyl were visualized in the complex with the amino acid residues of (GLY62, GLU159, LEU59, PRO221, LEU65, ARG111, PRO167, LEU65, LEU166, ILE217, PHE69) showed in Fig. 2. **A7** as a ligand compound expressed (−10.5 kcal/mol) binding affinity with the targeted modeled QcrB protein. Complex showed one Carbon Hydrogen Bond with the amino acid residue of (HIS216 at a distance of 3.78978 Å) and three different types of bonds such as Halogen
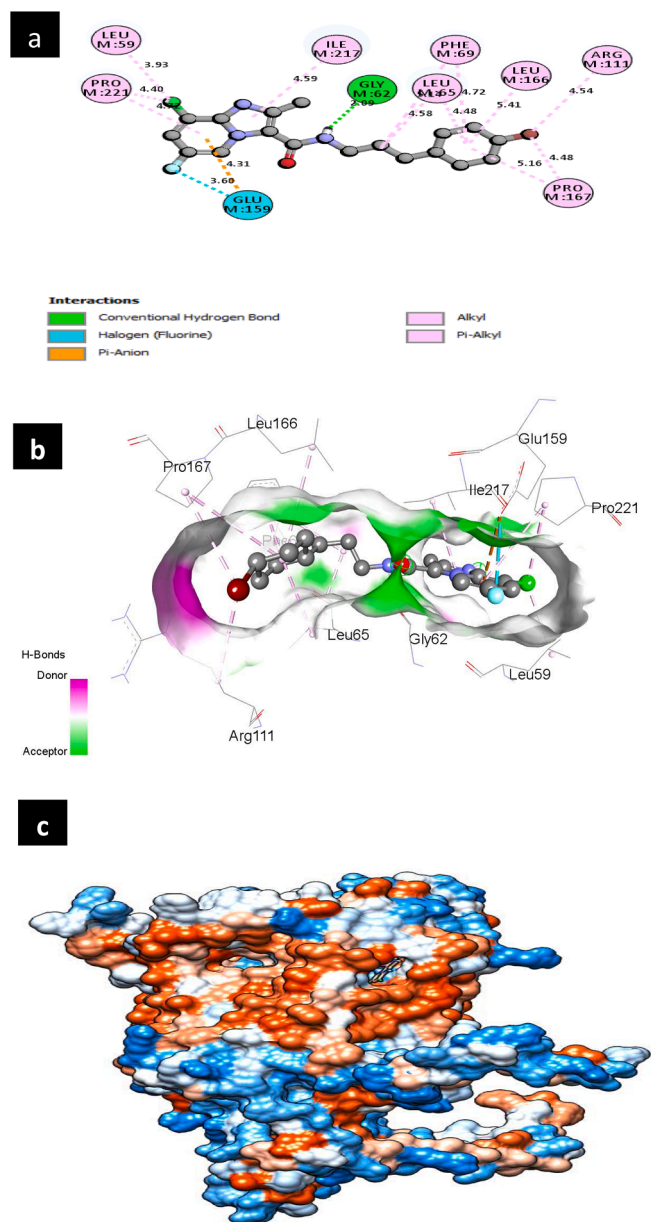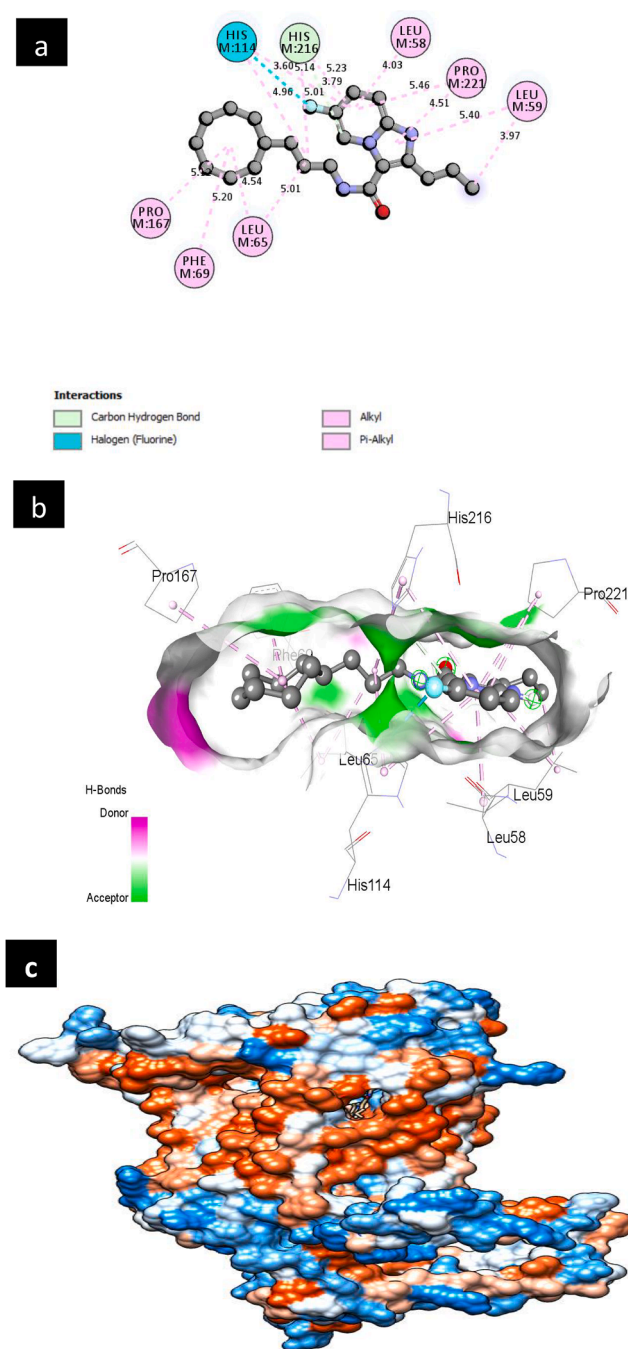
Fig. 2. (a) Schematic representation of predicted **A2** ligand with protein complex interactions in the 2D diagram. Interactions are colored depending on their type. (b) The three-dimensional representation of the binding pose, interactions, H bond donor, and acceptor surface of predicted **A2** ligand with protein complex. (c) Targeted protein is depicted in surface view and **A2** ligand compound as a stick in the binding pocket.

(Fluorine), Alkyl, Pi-Alkyl with the amino acid residues of (HIS114, LEU58, LEU59, LEU65, PRO167, PRO221, LEU59, PHE69, HIS114, HIS216) showed in Fig. 3. Furthermore, **A3, A4, A5, A8** ligand molecules as complexes with the targeted modeled QcrB protein also revealed higher binding affinity than the template molecule and standard drug respectively. Based on the highest molecular docking scores as binding affinity, non-bond interactions and in comparison with the binding affinity of the standard drug, three ligand compounds (**A6, A2, and A7**) were considered for further analysis.

3.2. ADME and toxicity prediction

Molecular weight (acceptable range: ≤500), number of hydrogen bond acceptors (acceptable range: ≤10), lipophilicity (Log P) ≤ 5, and

Fig. 3. (a) Schematic representation of predicted **A7** ligand with protein complex interactions in the 2D diagram. Interactions are colored depending on their type. (b) The three-dimensional representation of the binding pose, interactions, H bond donor, and acceptor surface of predicted **A7** ligand with protein complex. (c) Targeted protein is depicted in surface view and **A7** ligand compound as the stick in the binding pocket.

molar refractivity (40–130) indicates the five rules of Lipinski, are crucial parameters for a successful drug candidate [20]. All the ADME parameters including drug-likeness, pharmacokinetic profile, and water solubility were analyzed for the selected ligand molecules showed in Table 3. All the ligand molecules as **A6, A2,** and **A7** revealed 0 violations in Lipinski rules, similar bioavailability, and a high rate of gastrointestinal absorption. Only the **A2** ligand molecule has glycoprotein permeability. Toxicity prediction was analyzed to determine the compounds were whether toxic or not. Predicted results were shown in Table 4. Determination of carcinogenicity and cytotoxicity of **A6, A2, A7** were

Table 3

ADME and drug-likeness parameters of the selected IPAs.

ID	MW (g/mol)	nHBD	nHBA	Log S	GA	CPY	BBB	Pgp	BA	Log Po/w	SA	nLV
A6	373.51	1	3	−6.41	High	CPY2 D6 inhibitor	Yes	No	0.55	5.24	3.46	0
A2	343.25	1	3	−5.17	High	CYP2D6 inhibitor, CYP3A4 inhibitor	Yes	Yes	0.55	2.95	3.82	0
A7	373.51	1	3	−6.41	High	CYP2D6 inhibitor	Yes	No	0.55	5.24	3.46	0

Key: Molecular weight (MW), Number of hydrogen bond donor (nHBD), Water solubility (Log S), gastrointestinal absorption (GI), CYP isoform inhibitor (CPY), blood-brain barrier permeant (BBB), P-glycoprotein substrate (Pgp), Bio-availability (B), consensus Log Po/w, Synthetic Accessibility (SA), Number of Lipinski violation (nLV).

Table 4

Toxicity prediction of the selected IPAs.

Compound	Carcinogenicity	Cytotoxicity
A6	Inactive	Inactive
A2	Inactive	Inactive
A7	Inactive	Inactive

predicted inactiveness (non-toxic).

4. Conclusion

As an extension of our previous work, this research adopted the in-silico approach in analyzing the binding profiling of some newly designed IPA compounds as potential hits of anti-TB candidates. The template scaffold (Ligand 26) was selected for the in-silico design strategy and ligand compounds (**A1**–**A8**) were designed which exhibited better binding affinities when compared with that of the scaffold template (6.8 kcal/mol) and isoniazid standard drug (6.00 kcal/mol). In addition, all docking results of designed ligands with the targeted protein showed binding affinities ranging from (−8.5 kcal/mol to −11 kcal/mol). The drug-likeness and pharmacokinetic profile prediction results for the selected ligands with higher binding affinities (**A6, A2, and A7**) showed zero violations of Lipinski rules with similar bioavailability, and high rate in gastrointestinal absorption, while toxicity parameters such as carcinogenicity and cytotoxicity were all predicted as non-toxic (inactiveness).

Ethical statement

Not applicable

CRediT authorship contribution statement

Mustapha Abdullahi: Conceptualization, Methodology, Data curation, Visualization, Investigation, Supervision, Writing - original draft. **Niloy Das:** Software, Visualization, Validation, Writing - review & editing. **Shola Elijah Adeniji:** Data curation, Formal analysis, Supervision. **Alhassan Kabiru Usman:** Investigation, Writing - review & editing. **Ahmad Muhammad Sani:** Writing - review & editing.

Declaration of Competing Interest

The authors declare that they have no known competing financial interests or personal relationships that could have appeared to influence the work reported in this paper.

References

[1] Duarte R, Aguiar A, Pinto M, Furtado I, Tiberi S, Lönnroth K, et al. Different disease, same challenges: social determinants of tuberculosis and COVID-19. Pulmonology 2021;27(4):338–44. https://doi.org/10.1016/j.pulmoe.2021.02.002.

[2] Visca D, Ong CWM, Tiberi S, Centis R, D'Ambrosio L, Chen B, et al. Tuberculosis and COVID-19 interaction: a review of biological, clinical and public health effects. Pulmonology 2021;27(2):151–65. https://doi.org/10.1016/j.pulmoe.2020.12.012.

[3] Abdul-Hammed M, Adedotun IO, Falade VA, Adepoju AJ, Olasupo SB, Akinboade MW. Target-based drug discovery, ADMET profiling, and bioactivity studies of antibiotics as potential inhibitors of SARS-CoV-2 main protease (sMpro). VirusDisease 2021;1–29. https://doi.org/10.1007/s13337-021-00717-z.

[4] Pethe K, Bifani P, Jang J, et al. Discovery of Q203, a potent clinical candidate for the treatment of tuberculosis. Nat Med 2013;19(9):1157–60. https://doi.org/10.1038/nm.3262.

[5] Jadhavar PS, Patel KI, Dhameliya TM, Saha N. Bioorganic Chemistry Benzimidazoquinazolines as new potent anti-TB chemotypes: design, synthesis, and biological evaluation. Bioorg Chem 2020;99(March):103774. https://doi.org/10.1016/j.bioorg.2020.103774.

[6] Dhameliya TM, Patel KI, Tiwari R, Vagolu SK, Panda D, Sriram D, et al. Synthesis, and biological evaluation of benzo [d] imidazole-2-carboxamides as new anti-TB agents. Bioorg Chem 2021;107:104538. https://doi.org/10.1016/j.bioorg.2020.104538.

[7] Wang A, Li V K, Li L, Liu H, Tao Z, Wang B, et al. Design, synthesis and biological activity of N-(2-phenoxy)ethyl imidazo[1,2-a]pyridine-3-carboxamides as new antitubercular agents. Eur J Med Chem 2019;178:715–25. https://doi.org/10.1016/j.ejmech.2019.06.038.

[8] Ko Y, Choi I. Putative 3D structure of QcrB from Mycobacterium tuberculosis cytochrome bc1 complex, a novel drug-target for new series of antituberculosis agent Q203. Bull Korean Chem Soc 2016;37(5):725–31. https://doi.org/10.1002/bkcs.10765.

[9] Pan Z, Wang Y, Gu X, Wang J, Cheng M. Refined homology model of cytochrome Bcc complex B subunit for virtual screening of potential anti-tuberculosis agents. J Biomol Struct Dyn 2020;38(16):4733–45. https://doi.org/10.1080/07391102.2019.1688196.

[10] Abdullahi M, Shallangwa GA, Ibrahim MT, et al. QSAR studies on some C-14urea tetrandrine compounds as potent anti-cancer agents against leukemia cell line (K562). J Turkish Chem Soc, Section A: Chem. 2018;5(3). 10.18596/jotcsa.457618.

[11] Abdullahi M, Uzairu A, Shallangwa GA, Mamza P, Arthur DE, Ibrahim MT. In-silico modelling studies on some C14-urea-tetrandrine derivatives as potent anti-cancer agents against prostate (PC3) cell line. J King Saud Univ – Sci 2020;32(1):770–9. https://doi.org/10.1016/j.jksus.2019.01.008.

[12] Abdullahi M, Elijah S. In-silico molecular docking and ADME / pharmacokinetic prediction studies of some novel carboxamide derivatives as anti-tubercular agents. Chemistry Africa 2020;3(4):989–1000. https://doi.org/10.1007/s42250-020-00162-3.

[13] Abdullahi M, Shallangwa GA, Uzairu A. In silico QSAR and molecular docking simulation of some novel aryl sulfonamide derivatives as inhibitors of H5N1 influenza A virus subtype. Beni-Suef Univ J Basic Appl Sci 2020;2(9):1–12. https://doi.org/10.1186/s43088-019-0023-y.

[14] Oduselu GO, Ajani OO, Ajamma YU, Brors B, Adebiyi E. Homology modelling and molecular docking studies of selected substituted benzo[d]imidazol-1-yl)methyl) benzimidamide scaffolds on plasmodium falciparum adenylosuccinate lyase receptor. Bioinform Biol Insights. 2019;13. 10.1177/1177932219865533.

[15] Mora Lagares L, Minovski N, Caballero Alfonso AY, Benfenati E, Wellens S, Culot M, et al. Homology modeling of the human p-glycoprotein (Abcb1) and insights into ligand binding through molecular docking studies. Int J Mol Sci 2020;21(11):4058. https://doi.org/10.3390/ijms21114058.

[16] Abdullahi M, Adeniji SE, Arthur DE, Haruna A. Homology modeling and molecular docking simulation of some novel imidazo[1,2-a]pyridine-3-carboxamide (IPA) series as inhibitors of Mycobacterium tuberculosis. J Genet Eng Biotechnol 2021;19(1):1–13. https://doi.org/10.1186/s43141-020-00102-1.

[17] Abdullahi M, Uzairu A, Shallangwa GA, Mamza P, Arthur DE, Ibrahim MT. In-silico modelling studies on some C 14 -urea-tetrandrine derivatives as potent anti-cancer agents against prostate (PC3) cell line. J King Saud Univ – Science 2020;32(1):770–9. https://doi.org/10.1016/j.jksus.2019.01.008.

[18] Daggupati T, Pamanji R, Yeguvapalli S. In silico screening and identification of potential gsk3β inhibitors. J Recept Signal Transd 2018;38(4):279–89. https://doi.org/10.1080/10799893.2018.1478854.

[19] Peele KA, Potla C, Srihansa T, et al. Informatics in medicine unlocked molecular docking and dynamic simulations for antiviral compounds against SARS-CoV-2: a computational study. Inf Med Unlocked 2020;19(March):100345. https://doi.org/10.1016/j.imu.2020.100345.

[20] Prottoy NI, Sarkar B, Ullah A, Hossain S, Boby AS, Araf Y. Molecular docking and pharmacological property analysis of antidiabetic agents from medicinal plants of bangladesh against type II diabetes: a computational approach. PharmaTutor 2019;7(9):6–15.